Independent Control of Multiple Degrees of Freedom Local Magnetic Actuators with Magnetic Cross-coupling Compensation

Bruno Scaglioni,[1] *Member, IEEE*, Nicola Fornarelli[2], Nicolo Garbin[3], *Student Member, IEEE*, Arianna Menciassi[4], *Senior Member, IEEE*, and Pietro Valdastri,[1] *Senior Member, IEEE*

***Abstract*— This paper tackles the problem of independent control of multiple degrees of freedom systems based on Local Magnetic Actuation (LMA). This is achieved by means of a modular disturbance rejection scheme, with the aim of enhancing the range of use of Multiple-DoF LMAs in dexterous surgical manipulators. An LMA actuation unit consists of a pair of permanent magnets, characterized by diametrical magnetization, acting as magnetic gears across the abdominal wall. In this study, the model of the LMA and the time-varying magnetic disturbances owing to the proximity of multiple units are discussed. Subsequently, the developed model is capitalized in order to establish a Kalman state observer for the purpose of developing a sensor-free endoscopic manipulator suited to infer the state of the internal side of the LMA. Afterwards, the same model is used to develop an adaptive feedforward compensator system, with the aim of balancing the magnetic torques acting on the LMAs from the neighbouring units in the case of unknown and frequency-varying sinusoidal disturbances. The effect of a magnetic shield, realized by means of *MuMetal* is also analyzed. The overall control system is modular with respect of the number of units and requires no centralized intelligence.**

The proposed scheme is subsequently validated by means of experiments performed on a benchtop platform, showing the effectiveness of the proposed approach. In particular, the proposed state observer presents an Root Mean Square Error (RMSE) ranging from 28 rpm to 47 rpm in the estimation of the rotational velocity of the internal magnet and a RMSE of 1.18 mNm to 1.41 mNm in the estimation of a load torque. The disturbance compensation system provides a reduction of 40 $\%$ to 50 $\%$ in the disturbance caused by interacting LMA units.

I. Introduction

The practice of Minimally Invasive Surgery (MIS) appeared in the late 1980's [1], [2]. Since then, substantial amounts of research has been performed in order to introduce robotics into the MIS medical practice. Despite the availability of several platforms, pioneered by the DaVinci (Intuitive Surgical [3]), robotic MIS still presents several limitations such as higher invasiveness [4], cost and design complexity. In recent years, many advances have been proposed [5], nonetheless, the actuation design is crucial in order to guarantee dexterity through the realization of several DoF, simultaneously containing volume and complexity.

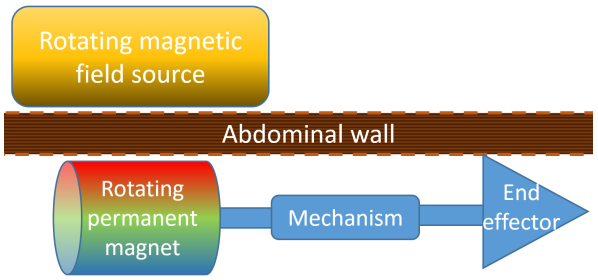

Fig. 1. Representation of the LMA concept, the torque is transmitted through the abdominal wall by means of a rotating magnetic field.

The actuation mechanism can be external, hence performed through rigid shafts or cables (e.g. [6], [7]), or internal, using on-board motors [8], smart materials [9] or other actuation strategies [10]. Internal actuation is certainly promising as the invasiveness is lower. Nevertheless, the main drawback of endo-actuated devices is the miniaturization of the actuating mechanism, as the volume reduction is inevitably associated with lower mechanical power. Among the possible strategies, magnetic actuation has the peculiarity of guaranteing coupling across the abdominal wall without the need of a dedicated entry port. For this reason, magnetic actuation is becoming popular in the surgical robotic field [11], [12].

Magnetic coupling as effective method for transmission of forces and torques in endoscopic devices has been recently implemented for propulsion of capsule robots [13], anchoring and motion of microrobots [14], and biopsy needles motion [15].

To address the problem of transmitting power to a miniaturized manipulator, the effectiveness of the LMA technique has been shown [16] while in [17] and [18] the implementation of LMA-based laparoscopic devices has been demonstrated. The LMA is based on the concept of *magnetic gears* [19], schematized in Fig. 1. An externally sourced magnetic field induces torque to a rotating permanent magnet placed inside the abdominal cavity. The rotating magnet acts as the actuation mechanism for a miniaturized surgical manipulator. Two approaches can be highlighted to generate the external magnetic field, electromagnetic (EM) sources or rotating external permanent magnets (EPM). In this work, the latter approach has been adopted. The closed loop

[1]{b.scaglioni,p.valdastri}@leeds.ac.uk, Storm Lab UK, School of Electronic and Electrical Engineering, University of Leeds, LS29JT, Leeds, UK

[2] Universita' di Pisa, 56126, Pisa, Italy

[3] nicolo.garbin.1@vanderbilt.edu, Mechanical Engineering department, Vanderbilt University. 37212 Nashville TN, USA

[4] arianna.menciassi@santannapisa.it, BioRobotics Institute, Scuola Superiore SantAnna, Pontedera (PI) 56025, Italy

The research reported in this article was supported in part by the Royal Society under grant number CH160052 and by the Engineering and Physical Sciences Research Council (EPSRC) under grant number EP/P027938/1. Any opinions, findings and conclusions, or recommendations expressed in this article are those of the authors and do not necessarily reflect the views of the Royal Society or the EPSRC.

control of a single-DoF, permament magnet actuated LMA is discussed in [20], although, a realistic manipulator based on the LMA would require many DoFs in order to achieve sufficient dexterity. Moreover, the amount of space in the abdominal cavity is limited. For this reason, multiple LMA units should be confined in a small volume to realize a multiple-DoF manipulator. Spatial proximity between LMAs would result in cross-magnetic disturbance acting between neighbouring DoFs. In [21] this problem is addressed for electromagnetic-actuated LMA in the case of one sinusoidal disturbance at constant frequency. This paper extends the results of [21] by adapting them to the case of permanent magnets and considering multiple disturbances at various and time-varying frequencies. The problem is initially tackled by adopting a physical shielding system and evaluating the effect on the performances of the single LMA. Subsequently, an independent control and compensation scheme for every DoF is developed, resulting in a modular system that can act as a base for the realization of LMA-based devices with multiple DoFs (an example is given in Fig. 2). The compensation scheme adopted here is valid for sinusoidal disturbances whose frequency evolves in time. Finally, this paper tackles the problem of adopting a sensorless approach for the LMA by inferring the status of the internal magnet from external measurements. A similar approach was adopted in [21], where the estimation was limited to the disturbance and not targeted at eliminating the sensors. The need for this approach is justified by the medical applications where the laparoscopic devices based on the LMA will undergo sterilization and difficult operational environments. Moreover, the absence of electrical components in the internal part of the laparoscopic device would result in a safer use and enhanced biocompatibility [17], [18].

In the following, all the magnetic DoFs are considered equal in size and shape, thus the mathematical model describing a single LMA will be considered. Initially, the interaction between the DoFs caused by magnetic cross-coupling will be neglected. Subsequently, the disturbances acting on the Internal Permanent Magnets (IPM) as a consequence of the magnetic interactions between DoFs will be considered.

The remainder of the paper is organized as follows. Section II describes the mathematical model of the single-DoF LMA and the model of the disturbances across different DoFs. Section III describes the control system architecture and the estimation method adopted to infer the state of the IPM, sensorless. In section IV the disturbance compensation scheme is discussed. In section V the techniques discussed earlier are validated on an experimental platform. Finally, in Section VI conclusions and future developments are discussed.

II. Mathematical model

A schematic representation of a multi-DoFs, LMA based, surgical manipulator, is shown in Fig. 2. The system is composed by a series of LMA units. External and internal magnets are different in size and are assumed to rotate about parallel axis. h is the intermagnetic distance between the

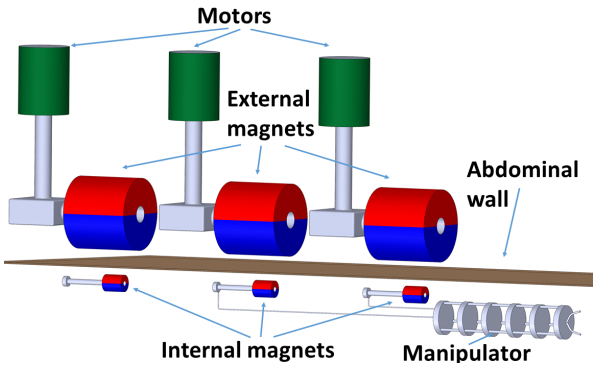

Fig. 2. Schematic representation of the relevant components of multiple LMA units.

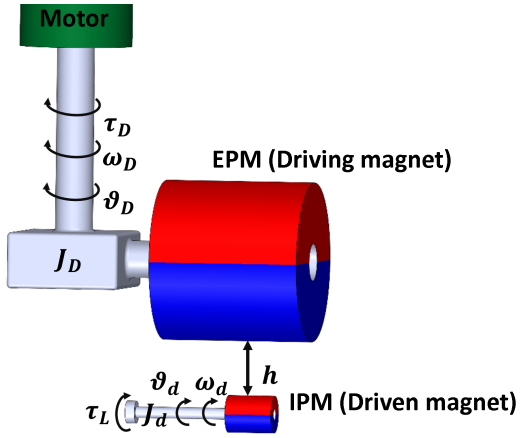

Fig. 3. Schematic representation of the single DoF LMA.

magnets. Although h can change depending on the anatomy of the patients and the specific application, it can be considered constant within a single procedure, and therefore easily tunable. In the considered setup, each External Permanent Magnet (EPM) is actuated by a dedicated DC electric motor connected to the magnet by means of a shaft, furthermore, the load acting on the internal permanent magnet is considered.

For the sake of simplicity, the model of the single DoF (represented in Fig. 3) will be initially considered, subsequently, the interactions between different DoFs will be added to the system. The electrical dynamics can be modelled as:

$$V_m = K_m \omega_D + R_m i_m + L_m \dot{i}_m, \tag{1}$$

where V_m is the voltage applied to the motor, K_m is the motor voltage constant, ω_D is the rotational velocity of the external assembly, R_m and L_m are the motor resistance and inductance, and i_m is the motor current.

The model of the magneto-mechanical dynamics is based on the discussion of [20]. The magnetic coupling is modelled as an asymmetrical spur gear pair where the transmitted torques are two different functions of the angle difference and the axial distance. In particular:

$$T_c^{Dd}(\Delta\theta, h) = T_{max}^{Dd}(h) sin(\Delta\theta), \tag{2}$$
$$T_c^{dD}(\Delta\theta, h) = T_{max}^{dD}(h) sin(\Delta\theta), \tag{3}$$

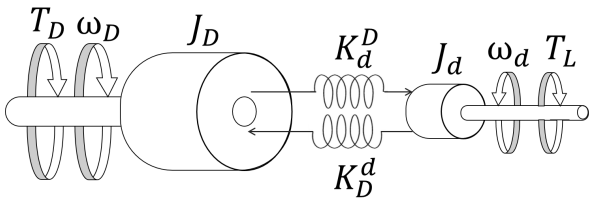

Fig. 4. Schematic equivalent model of the single DoF LMA, [20].

where $\Delta\theta$ is the angular displacement of the two rotating magnets, i.e. $\Delta\theta = (\pi + \frac{\pi}{2} - |\theta_D| - |\theta_d|)$, θ_D and θ_d being the angular positions of the EPM and IPM respectively. The first π is motivated by the attraction of opposite poles, while the $\frac{\pi}{2}$ arises because torque is transmitted between the magnets when the relative angle is near to $\frac{\pi}{2}$. As a consequence, if the magnets are rotating with the same angular velocity and transmitting torque, $\Delta\theta$ can be considered to be in the proximity of zero. Conversely, if $\Delta\theta$ increases, the load torque overcomes the transmitted torque and the control on the system is lost, leading to a *pole slipping* condition. When the system is in a controlled state, T_c^{Dd} and T_c^{dD} can be approximated, for a given h, as constant values of K^{Dd} and K^{dD}, respectively. Moreover, T_{max}^{Dd} and T_{max}^{dD} are the maximum transmittable torques, function of the distance h. Numerical values of T_{max}^{Dd} and T_{max}^{dD} for different values of h can be computed by means of finite element simulations.

The simplified model of the single LMA, represented in Fig. 4 is:

$$J_D\dot{\omega}_D = \tau_D - K^{Dd}\Delta\theta \quad (4)$$

$$J_d\dot{\omega}_d = K^{dD}\Delta\theta + \tau_L \quad (5)$$

where τ_D is the driving torque, $\dot{w}_D$, $\dot{w}_d$, J_D and J_d are the time derivatives of the rotational velocities and the rotational inertias of the EPM and IPM respectively.

By recalling that the driving torque τ_D is proportional to i_m through the motor torque constant K_τ and combining eqs. 1, 4 and 5, the complete system can be written in state-space form as:

$$\dot{\theta}_D = \omega_D, \quad (6)$$

$$\dot{\theta}_d = \omega_d, \quad (7)$$

$$\dot{i}_m = \frac{1}{L}(V_m - K_m\omega_D - R_m i_m), \quad (8)$$

$$\dot{\omega_D} = \frac{1}{J_D}(-K^{dD}\theta_D + K^{dD}\theta_d + K_\tau i_m) - \frac{1}{J_D}(C_{fD}\omega_D) \quad (9)$$

$$\dot{\omega}_d = \frac{1}{J_d}(K^{Dd}\theta_D - K^{Dd}\theta_d - \tau_L - C_{fd}\omega_d) \quad (10)$$

Two additional terms in the torque balance equations have been added in order to take into account the rotational friction of the external and internal shaft. It must be pointed out that the system described by eqs. (6-10) is linear (assuming the approximation of a small $\Delta\theta$), although, it contains electrical and mechanical dynamics, hence the numerical integration of such system is challenging (i.e. the problem is stiff), moreover, the different dynamics naturally recall for a two time-scales control.

A. Cross-coupling modelling

In [21], a model of cross-disturbances is proposed for electro-magnetically actuated LMA (LEMAs). In the context of this paper, a similar approach is adopted and extended for multiple DoFs. The magnetic interference induced on the IPMs by magnetic coupling relative to the other DoFs is acting on each IPM as an input torque disturbance. The disturbance induced on the internal magnets is considered as a function of the difference of the velocities, i.e.: $d(t) = K_{dist}sin(\omega_{diff}t + \Phi)$ where K_{dist} is as unknown coefficient describing the intensity of the coupling, and ω_{diff} is defined as the difference between the two angular velocities, i.e.: $\omega_{diff} = |\omega_{dof1} - \omega_{dof2}|$. The approach is here generalized to multiple DoFs and adapted for the LMA system with external permanent magnets. The model of the disturbance acting on the i^{th} IPM is defined as:

$$d(t)^i = \sum_{\substack{j=1 \\ j\neq i}}^{N} K_{dist}^{ji}(\omega_{diff}^{ji})sin(\omega_{diff}^{ji}t)\,, \quad (11)$$

where N is the total number of interacting DoFs, K_{dist}^{ji} represents the coupling between the j^{th} LMA unit and the i^{th} IPM at a specific ω_{diff}^{ji}, and ω_{diff}^{ji} is defined as the difference between the velocity of the j^{th} EPM and the velocity of the i^{th} IPM. The disturbance defined in eq. (11) is assumed to act as an input torque on the i^{th} internal magnet, having no direct effect on the external magnet. This assumption holds true if $J_D^i \gg J_d^i$, as the inertia of the EPM operates as a low-pass filter, reducing the amplitude of the disturbance to a negligible value. It must be pointed out that, in the scope of the applications for which the LMA system is designed, the assumption of $J_D^i \gg J_d^i$ is widely satisfied, as the functional requirements limit the size of the IPM, while the size of the EPM is directly related to the magnitude of K^{Dd_i} and K^{dD_i}, hence, to the amount of transmittable torque. Moreover, the inertia of the EPM is a stabilizing factor in torque transmission, although an increased inertia would result in an increased energy consumption during operation.

In the context of this paper, the effect of physical shielding with *MuMetal* is also considered. The shielding is adopted in order to minimize the effect of the disturbances, thus reducing the $K_{dist}^{ji}(\omega_{diff}^{ji})$ term of eq. (11). The adoption of a physical shielding for reduction of magnetic cross-disturbances is a natural choice. Moreover, the contraction of $K_{dist}^{ji}(\omega_{diff}^{ji})$ would result in a smaller control action for a control-based disturbance compensator, regardless of the compensator design. Conversely, the adoption of a physical shield would negatively affect the total transmittable torque within the magnetic gear, namely K^{Dd_i} and K^{dD_i}. The analytical modelling of the aforementioned effects is an intricate question as it is influenced by the magnetic permeability of the shielding material, along with the geometry of the shielding and the distance from the gears. In order to tackle

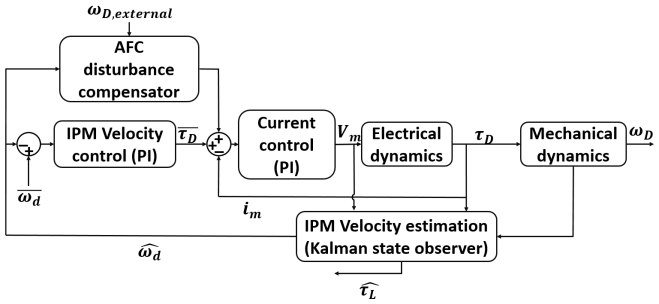

Fig. 5. Scheme of the LMA control system.

this problem, an additional term in the definition of T_{max}^{Dd} and T_{max}^{dD} will be introduced, as follows:

$$T_{max}^{Dd} = T_{max,U}^{Dd} - T_{lost} \quad (12)$$
$$T_{max}^{dD} = T_{max,U}^{dD} - T_{lost} \quad (13)$$

where $T_{max,U}^{Dd}$ and $T_{max,U}^{dD}$ are the maximum transmittable torques without shielding, and T_{lost} is the term describing the loss due to the presence of the shield.

The mathematical form of T_{lost} will be defined as a consequence of the experimental observations, as described in Section V. It must be pointed out that the term $K_{dist}^{ji}(\omega_{diff}^{ji})$ will be considered unknown in the following, consequently, an experimental characterization of this term is beyond the scope of the paper.

III. Control system architecture

The electro-mechanical nature of the LMA system summons to a multi-layer control scheme, the overall diagram of the control system is depicted in Fig. 5. Every DoF is autonomously controlled by a two-layer system. The inner layer controls the torque produced by the motor (τ_D) by regulating the current through a Proportional-Integral (PI) controller. By closing a current loop at high frequency, it is possible take into account the low-frequency approximation of the system by neglecting the electrical dynamics and considering uniquely the magneto-mechanical dynamics. A second PI controller is closing the velocity loop, this control scheme is well-known in literature as cascade control. A position loop is not considered here as any application would introduce a slowly moving load, and consequently a high-ratio transmission gear as in [17]. In this context, it would be more convenient to close the position loop on the load. The system's dynamics are varying with respect to the intemagnetic distance h, hence, an optimized velocity controller could be synthesized. Nevertheless, the requirements of the control system in terms of disturbance rejection are not strict, and a dedicated disturbance compensator will be described in Section IV. For these reasons, it is convenient to define a single PI controller (e.g. through the Ziegler-Nichols method) for an intermediate distance h and verify the stability margin of the closed loop system for the other intermagnetic distances under investigation.

It must be pointed out that the velocity loop can be closed on ω_D or ω_d. In the first case, the synthesis of the controller is trivial and the achievable bandwidth is very high, but the controller will be less sensitive with respect to the real velocity of the IPM. Conversely, closing the loop on ω_d requires a reliable measurement of the IPM velocity. Functional requirements like biocompatibility, the aptitude for sterilization, or the general indication of maintaining the design of the internal component of the system as simple as possible, might limit the chance to directly measure the IPM velocity, leading the way to the development of an estimation system of unmeasurable quantities. A possible approach is described in the following.

A. Estimation of the IPM velocity and torque load

The system described by eqs. (6-10) can be considered as a Multiple Input Multiple Output (MIMO) linear system where V_m and τ_L are inputs, the state vector is $x = [\theta_D, \theta_d, i_m, \omega_D, \omega_d]^T$ and the measurable part of the state is $y = [i_m, \theta_D, \omega_D]$, while the measurable input is $u = [V_m]$. For the purpose of estimating ω_d on such kind of a linear system, it is straightforward to build a *Kalman state observer*, provided that the system is observable and asymptotically stable. Depending on the coefficients, the system might show ill-conditioned matrices, due to the presence of electrical and mechanical dynamics. For this reason, the observability of the system has been proven by computing the gramian matrix, which is positive definite and shows numerical results which are more roboust to ill-conditioning with respect to the classical observability criterion. Moreover, it is possible to estimate the load torque acting on the IPM, by means of the Unknown Input Observer (UIO) technique [22], combined with the Kalman state observer. The well-known kalman estimator gives an optimal solution to the problem of finding the matrix L such that:

$$\hat{x} = A\hat{x} + Bu + L(y - C\hat{x}) \quad (14)$$

where A, B and C are the state space matrices of the linear system, and $\hat{x}$ is the estimated state vector. In order to estimate the unknown load torque τ_L, the input is considered as an additional state variable such as:

$$\dot{z} = A_f z \quad (15)$$
$$\tau_L = C_f z \quad (16)$$

and the state vector is augmented to accomodate the estimation of z. Further details on the UIO can be found in [23]. By adopting this approach, eq. (14) turns:

$$\begin{bmatrix}\dot{\hat{x}} \\ \dot{\hat{z}}\end{bmatrix} = \begin{bmatrix}A & BC_f \\ 0 & A_f\end{bmatrix}\begin{bmatrix}\hat{x} \\ \hat{z}\end{bmatrix} + \begin{bmatrix}B \\ 0\end{bmatrix} - L(y - C\hat{x}) \quad (17)$$
$$\hat{\tau_L} = C_f\hat{z} \quad (18)$$

The simplest form of UIO makes no assumption on the dynamics of the unknown input, hence $C_f = 1$ and $A_f = 0$. A further assumption can be made if A_f is assumed to be a real and negative scalar $A_f = -c_l$. In the context of this paper, the most conservative approach is adopted,

consequently, no assumptions on the load dynamics have been made. The augmented system including the unknown input is linear, thus an augmented Kalman observer can be computed. Provided that the observer is much faster than the system, the estimated ω_d can be used to close the velocity loop without the need of sensors on the IPM, thus providing a solution for a lighter and more functional LMA actuator. In order to compute the Kalman observer, the covariance matrices of the measurement and process noise (usually R and Q, respectively) are required. Although it is quite easy to compute R from measurements, the Q matrix represents a measurement of how much the process deviates from the nominal model. This is often tuned by means of heuristics, the same approach has been adopted in this paper.

IV. Time varying disturbance rejection

As described in sec. II the dynamic model of the single DoF LMA is linear, but the magnetic cross-coupling affecting the IPMs is a sinusoidal function of ω_{diff}^{ji} for the i^{th} internal magnet. This introduces a nonlinear, time varying term in eq. (10) that depends on the states of other DoFs. In practice, K_{dist}^{ji} is going to be negligible for most inter-DoF coupling, nevertheless, neighbour DoFs could recieve a significant amount of disturbance. The aforementioned disturbances can be compensated by an Adaptive Feedforward Compensator (AFC) system [24]. This technique is widely adopted in noise compensation and disturbance compensation on rotating devices (e.g. compact discs) as it involves the addition of an adaptive feedforward term that does not require any change in the closed loop control system. For the sake of simplicity, the case of a disturbance generated by a single degree of freedom j on the i^{th} IPM is discussed. It must be pointed out that this implies no loss of generality, as the proposed approach can be scaled up to a generic amount of sinusoidal, time varying disturbances. The disturbance rejection problem can be formulated as:

$$y(t) = g_d(t) * [u_c(t) - d(t)] \tag{19}$$

where $g_d(t)$ is the impulse response of the single LMA which can be easily obtained as a high frequency approximation of eqs.(6-10), $*$ denotes the convolution operation, $u_c(t)$ is the compensating input (superposed to the input coming from the closed loop regulator) and $d(t)$ is the disturbance. The goal of the compensator is to generate a $u_c(t)$ such that $y(t) \to 0$ as $t \to \infty$ Considering a single disturbance in the form described by eq.(11) as:

$$d(t) = K_{dist}(\omega_{diff}) sin(\alpha(t)) \tag{20}$$

$$\frac{d\alpha_d(t)}{dt} = \omega_{diff}(t) \tag{21}$$

where $K_{dist}(\omega_{diff})$ is considered unknown, and $\alpha(t)$ is the integral of the disturbance frequency ω_{diff},i.e. the difference in angular position between the magnets, one can assume a control input in the form:

$$u_c(t) = K_{comp}(t) sin(\alpha_d(t)). \tag{22}$$

The complete disturbance compensation would be exactly achieved by letting $K_{comp}(t) = K_{dist}(\omega_{diff}(t))$. Being $K_{dist}(\omega_{diff})$ unknown, an appropriate parameter adaptation strategy would asymptotically allow the compensation goal to be reached. Algorithms defining the adaptation strategy fall into the framework of adaptive control theory [25]. The simplest algorithm is the *pseudo gradient algorithm*, simply given by:

$$\frac{dK_{comp}}{dt} = -g\omega_{diff} y(t) \tag{23}$$

where $g > 0$ is the adaptation gain. Adaptive control theory guarantees Lyapunov stability for such kind of systems only if the Laplace transform of $g_d(t)$ is *strictly positive real*, which is rarely satisfied in practice. However, [24] has demonstrated the equivalence of such adaptive compensation system with respect to a Linear Time Variant (LTV) controller with state space realization:

$$\dot{x_c}(t) = A_d(t) x_c(t) - \begin{pmatrix} 0 & -g \end{pmatrix}^T y(t) \tag{24}$$

$$u(t) = C_d x_d(t) \tag{25}$$

where

$$A_d(t) = \begin{bmatrix} 0 & \omega_{diff}(t) \\ -\omega_{diff}(t) & 0 \end{bmatrix}, \quad C_d = \begin{pmatrix} 0 & 1 \end{pmatrix} \tag{26}$$

As the parameter $\omega_{diff}(t)$ appears linearly in eq.(26), the closed loop system is a Polytopic Linear Parameter Varying system (PLPV), for which the stability can be guaranteed if there exists a single positive definite matrix P such that:

$$M_i^T P + P M_i < 0, \quad i = 1, 2 \tag{27}$$

where M_1 and M_2 are the state space matrices relating the states to the derivatives of the closed loop system in the cases of minimum and maximum disturbance frequencies, respectively. Eq.(27) can be solved using a *linear matrix inequality* solver [26]. Being M relative to the close loop system, the adaptation gain g appears in it [24], hence, it is possible to use eq.(27) to compute the maximum g such that the system is stable.

Despite the proposed formulation being developed for the rejection of a single, time-varying sinusoidal disturbance, it is straightforward to increase the number of independent compensation subsystem, although, the disturbances on the i^{th} DoF are likely to have relevant magnitude only from the neighbouring DoF, usually $(i-1)^{th}$ and $(i+1)^{th}$. It must be mentioned that the compensation system is decentralized as one or more compensators can be established for all the DoFs independently. The only external information required are the velocities of the other DoFs, which, due to the magnitude of the magnetic couplings and particularly in the case the DoFs are shielded, can be approximated with the velocities of the EPMs.

V. Simulations and experiments

The techniques proposed in Sections III and IV have been validated by means of experiments. The experimental platform is represented in Fig. 6. The motor used to spin the EPM is a DC Motor (148867, Maxon Motor, Sachseln,

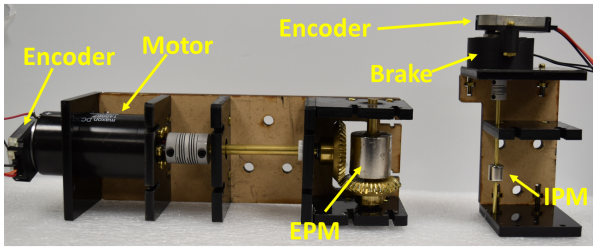

Fig. 6. Single DoF LMA experimental platform.

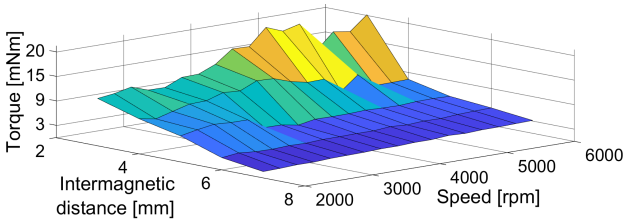

Fig. 7. Load torque required to enter the poles slipping condition without shielding.

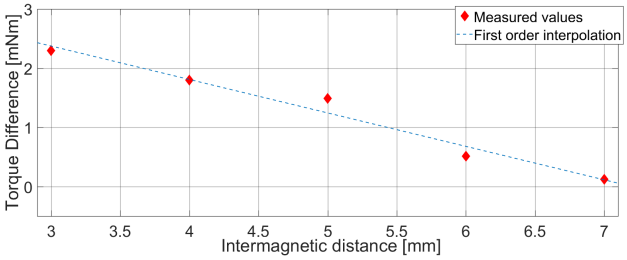

Fig. 8. Effects of physical shielding with *MuMetal*: Average difference between maximum torque transmission with unshielded and shielded LMA at various distances.

Switzerland), able to produce 190 mNm of torque and a maximum speed of 7000 rpm. Two rotary encoders have been applied on the external and internal magnets, which are both NdFeB N42 grade magnets, with 25.4 mm and 9.5 mm diameters respectively.

As mentioned in Section III, the diameter of the internal magnet is limited by the functional requirements, hence, it has been chosen to adopt a magnet able to enter an abdominal cavity through a standard 12 mm laparoscopic incision. An hysteresis brake was adopted to simulate the presence of a varying load torque. The current control loop is carried out by a microcontroller at 20 kHz. The velocity loop, the observer and the AFC are run on a desktop PC at 1 kHz. Regarding the values of $T^{Dd}_{max}(h)$ and $T^{dD}_{max}(h)$, the same magnets have been adopted in [20], hence the same numerical values have been used here, i.e.:

$$T^{Dd}_{max}(h) = (78e^{-105h} + 12e^{-31h})10^{-3} \quad (28)$$
$$T^{dD}_{max}(h) = (222e^{-169h} + 63e^{-51h})10^{-3} \quad (29)$$

where the intermagnetic distance h is expressed in meters. Initially, the effect of physical shielding has been investigated in order to compute the value of $T_{lost}(h)$. Three sheets of high magnetic permeability alloy (MuMetal, Carpenter Technology Corp., USA), offering a permeability of $3.5 \cdot 10^5$ H/m to $5 \cdot 10^5$ H/m have been added on the lateral sides of the system. In order to show the effect of shielding, the stall torque, defined as the required torque in order to have poles slipping, and consequently a loss of control on the velocity of the IPM, has been recorded. Fig. 7 shows the torque required to enter the pole slipping condition without shielding, the intermagnetic distance h, ranging from 3 to 7 cm with 1 cm interval is reported on the X axis, the EPM velocity, ranging from 1500 to 7000 rpm with increments of 500 rpm is on the Y axis, while on the Z axis the braking torque is reported. It must be pointed out that, in the previous paper on closed loop control of a similar platform [20], only speeds up to 1700 rpm were considered, while in the present work speeds up to 7000 rpm are reported. The maximum transmittable torque is decreasing with distance. Interestingly, also the variability of the torque is significantly decreasing with distance. This can be explained by the fact that the rotation of the IPM is smoother when the magnetic attraction force between the magnets is reduced. Moreover, at higher speeds the smoothness of the system's motion entails the torque to be lower. In Fig. 8, the effect of the shielding with *MuMetal* is represented, the average difference in transmittable torque between the unshielded and shielded condition are shown, depending on the intermagnetic distance h. The influence of the shielding on the torque transmission is always present, moreover, it significantly reduces with distance. The measured data have been interpolated with a first order polynomial whose coefficients have been used to shape the T_{lost} term. It must be mentioned that the effect of shielding is always below 2.5 mNm, which is small with respect to T^{Dd}_{max} and T^{dD}_{max}. The effect of shielding on the torque transmission can be considered acceptable.

The validation of the IPM velocity and load torque estimations have been carried out by means of dedicated experiments. In order to validate the speed estimation, a varying velocity setpoint has been given to the IPM, at different intermagnetic distances (namely 3, 5 and 7 cm). The measured speed has been compared to the output of the oberserver. Fig. 9 shows the estimated and measured IPM velocities for an intemagnetic distance of $h = 5$ cm. The dashed red curve is the IPM velocity setpoint, while the full blue and green lines represent the estimated and measured speed respectively. The estimated speed is in perfect accordance with the measurement, showing a good performance of the Kalman state observer in terms of estimating ω_d. In order to quantify the quality of the estimation, the root mean square error (RMSE) between the measured and estimated signals have been computed, resulting in 28.21, 37.23 and 45.43 rpm for $h = 3, 5, 7$ cm respectively. It must be mentioned that the state observer described here exibits a dependency on the intermagnetic distance h. Some experiments have been carried out to explore the robustness of the observer with respect to this parameter. The performances of an observer designed for a given $h = h_1$ turned out to be unsatisfactory in case $h \neq h_1$. For this reason, further work can be carried

out to design an adaptive Kalman observer. However, the distance h can be assumed to be quasi-constant in the context of laparoscopic applications, hence, an LTI observer can be computed prior to every use of the platform. Fig. 10 shows the load torque (τ_L) estimation when a sinusoidal load torque is applied to the system and the speed of the IPM is simultaneously controlled to a constant value. A sinusoidal load torque with varying frequency (0.35, 0.6 and 0.8 Hz) and an average value of 8 mNm and an semi-amplitude of 3 mNm is applied. The amplitude of the load torque has been chosen in order not to reach the amount of torque available at the considered intermagnetic distance, but simultaneously to significantly affect the dynamics of the system. Measurements have been taken with constant IPM speeds of $\omega_d = 2500$ and $\omega_d = 4000$ rpm, although, only the case of $\omega_d = 4000$ rpm is shown in Fig. 10. The RMSE of the difference between applied and estimated load torque has been computed, resulting in 1.41 and 1.18 mNm, for $\omega_d = 2500$ and $\omega_d = 4000$ rpm, respectively. The quality of the results for this experiment is lower with respect to the estimation of the IPM speed. As shown by 10, load torques with greater frequencies can be estimated with lower accuracy. This can be attributed to the absence of any assumption on the disturbance dynamics. Further improvements in terms of performances could be achieved by adopting assumptions on the form of A_f, although, suitable assumptions are context-dependent and could be expressed depending on the considered application.

These results opens the way for more complex control algorithms in LMA applications. E.g. in the case of tissue retraction [17] or motion of a laparoscopic camera [18], it would be possible to estimate the wrench applied to the tissue, or the stress in the structure of the controlled mechanism, and apply consequent control actions.

The validation of the disturbance compensation system has been carried out by introducing an additional LMA unit in the experimental setup. The additional DoF has been placed at a fixed distance from the IPM, i.e. 10 cm. In order to show the effectiveness of the compensator, the physical shield has not been considered.

The ω_d signal has been recorded in three scenarios: with the second EPM switched off, with the second EPM switched on, and finally with the compensation system activated. The experiment has been repeated for $\omega_d = 1000$ rpm, with the second EPM rotating at $\omega_{dist} = 1500$ rpm and $\omega_{dist} = 1800$ rpm, and 2000 rpm, with the second LMA unit rotating at $\omega_{dist} = 2500$ rpm. It must be pointed out that, in practice, only small differential speeds affect the system, as the inertia of the rotating components naturally filters high frequencies. For this reason, only ω_{diff}, equal to 500 rpm and 800 rpm have been considered. The adaptation gain, described in eq. (23) has been computed by means of eq. (27). Moreover, the compensation term of the control action $u_c(t)$ has been limited to a current of 1 A in order to avoid the saturation of the DC motor. It must be pointed out that the signal representing the rotational velocity of the IPM is particularly noisy, hence, results will be shown in the frequency domain,

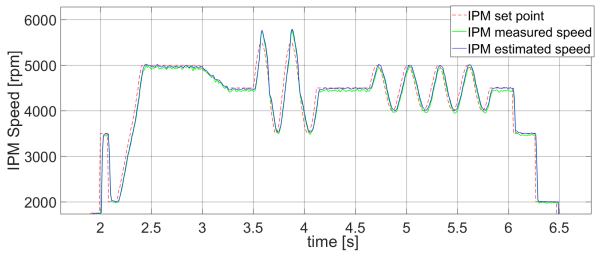

Fig. 9. Comparison between measured and estimated IPM speed.

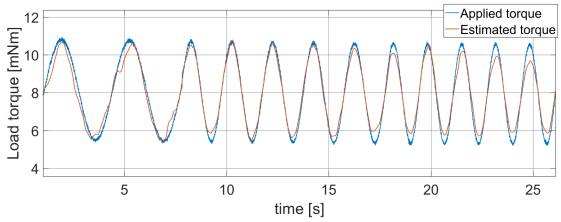

Fig. 10. Comparison between measured and estimated load torques, $\omega_d = 4000$ RPM.

where the disturbance and compensation effects are clearly visible. Fig. 11 shows the experimental results in the three scenarios described above. In the left column, a comparison between the Fast Fourier Transform (FFT) of the IPM velocity with no disturbances (blue) and with disturbances (red) is shown, the second column shows the comparison between the non compensated and the compensated cases. In cases (A) and (C) the disturbance frequency is 8.33 Hz (due to a differential velocity of 500 rpm), while in case (B), the disturbance frequency is 13.33 Hz.

The effect of the disturbance is clearly visible in the red line, moreover, in cases (A) and (B) a component around 17 Hz, due to the rotational frequency of the IPM, is visible. The right column shows the effect of the active disturbance compensator. The non compensated signal (red) is compared to the case where the AFC is active (green). In all the considered scenarios, the frequency component related to the disturbance is reduced by more than half. In particular, case (A) shows an amplitude reduction of the peak of 51.2 %, case (B) shows a reduction of 56.9 % and case (C) shows a reduction of 50.9 % The disturbance is not completely compensated, this can be explained by a conservative choice of the adaptation gain and by the saturation of the actuator. Moreover, it must be pointed out that the assumption of purely sinusoidal disturbance is strict in the case of an experimental platform. However, the adopted compensation scheme has shown good performances in a real scenario.

VI. Conclusions

In this paper, a comprehensive control scheme for multiple LMA units has been proposed. The effect of physical shielding on the transmittable torque is shown to be acceptable in terms of performance loss. Subsequently, a disturbance compensation scheme, valid for multiple frequencies and scalable to the number of DoFs, has been proposed and experimentally validated. Moreover, a possible approach for

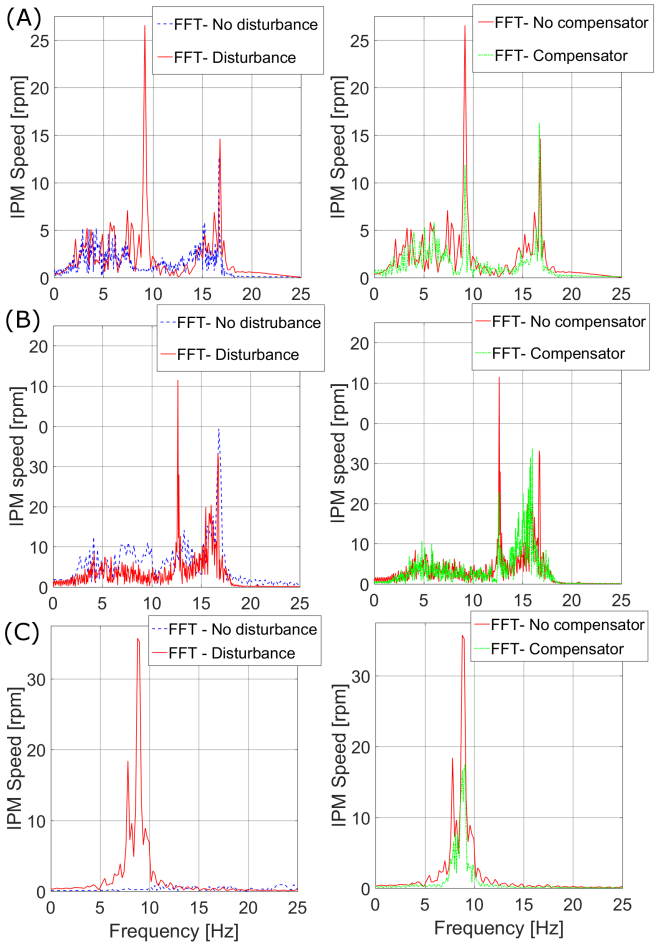

Fig. 11. Comparison between active and inactive disturbance left column and active / inactive compensation (right column). Three scenarios are taken into account: (A) $\omega_d = 1000\ rpm$ and $\omega_{dist} = 1500\ rpm$, (B) $\omega_d = 1000\ rpm$ and $\omega_{dist} = 1800\ rpm$ and (C) $\omega_d = 2000\ rpm$ and $\omega_{dist} = 2500\ rpm$. On the left the FFT of the IPM velocities when the disturbance is not active (dashed blue) and when the disturbance is active (red). On the right the comparison between the case with no compensation (red) and active compensator (dashed green).

the system control, avoiding the need for sensors on the internal side of the system, has been discussed. The proposed approach could be adopted for the control and compensation of sinusoidal disturbances in other applications based on multiple rotating magnetic fields. Future works will include the adoption of the discussed strategies in the development of a LMA-based laparoscopic manipulator.

REFERENCES

[1] W. S. Richardson, K. M. Carter, G. M. Fuhrman, J. S. Bolton, and J. C. Bowen, "Minimally invasive abdominal surgery." *The Ochsner journal*, vol. 2, no. 3, pp. 153–7, 2000.

[2] A. G. Harrell and B. T. Heniford, "Minimally invasive abdominal surgery: Lux et veritas past, present, and future," *American Journal of Surgery*, vol. 190, no. 2, pp. 239–243, 2005.

[3] "Intuitive Surgical", "DaVinci Surgical System."

[4] F. Kockerling, "Robotic vs. Standard Laparoscopic Technique-What is Better?" *Frontiers in Surgery*, vol. 1, pp. 10–13, may 2014.

[5] B. J. Nelson, I. K. Kaliakatsos, and J. J. Abbott, "Microrobots for Minimally Invasive Medicine," *Annual Review of Biomedical Engineering*, vol. 12, no. 1, pp. 55–85, 2010.

[6] J. Ding, R. E. Goldman, K. Xu, P. K. Allen, D. L. Fowler, and N. Simaan, "Design and Coordination Kinematics of an Insertable Robotic Effectors Platform for Single-Port Access Surgery," *IEEE/ASME Transactions on Mechatronics*, vol. 18, pp. 1612–1624, 2013.

[7] "Past, Present, and Future of Minimally Invasive Abdominal Surgery," *Journal of the Society of Laparoendoscopic Surgeons*, vol. 19, no. 3, 2015.

[8] A. C. Lehman, N. A. Wood, S. Farritor, M. R. Goede, and D. Oleynikov, "Dexterous miniature robot for advanced minimally invasive surgery," *Surgical Endoscopy and Other Interventional Techniques*, vol. 25, no. 1, pp. 119–123, 2011.

[9] H. Adldoost, B. R. Jouibary, and A. Zabihollah, "Design of SMA micro-gripper for minimally invasive surgery," *2012 19th Iranian Conference of Biomedical Engineering, ICBME 2012*, pp. 97–100, 2012.

[10] H. M. Le, T. N. Do, and S. J. Phee, "A survey on actuators-driven surgical robots," *Sensors and Actuators, A: Physical*, vol. 247, pp. 323–354, 2016.

[11] F. Leong, N. Garbin, C. D. Natali, A. Mohammadi, D. Thiruchelvam, D. Oetomo, and P. Valdastri, "Magnetic surgical instruments for robotic abdominal surgery," *IEEE Reviews in Biomedical Engineering*, vol. 9, pp. 66–78, 2016.

[12] L. Sliker, G. Ciuti, M. Rentschler, and A. Menciassi, "Magnetically driven medical devices: A review," *Expert Review of Medical Devices*, vol. 12, no. 6, pp. 737–752, 2015.

[13] A. Z. Taddese, P. R. Slawinski, K. L. Obstein, and P. Valdastri, "Closed Loop Control of a Tethered Magnetic Capsule Endoscope," *Robotics: Science and Systems XII*, vol. June, pp. 1139–1144, 2016.

[14] G. Tortora, P. Dario, and A. Menciassi, "Array of robots augmenting the kinematics of endocavitary surgery," *IEEE/ASME Transactions on Mechatronics*, vol. 19, no. 6, pp. 1821–1829, 2014.

[15] L. Huang, L. Rogowski, M. J. Kim, and A. T. Becker, "Path Planning and Aggregation for a Microrobot Swarm in Vascular Networks Using a Global Input," in *2017 IEEE/RSJ International Conference on Intelligent Robots and Systems (IROS)*. IEEE, Sept. 2017, pp. 414–420.

[16] C. Di Natali, T. Ranzani, M. Simi, A. Menciassi, and P. Valdastri, "Trans-abdominal active magnetic linkage for robotic surgery: Concept definition and model assessment," *Proceedings - IEEE International Conference on Robotics and Automation*, pp. 695–700, 2012.

[17] N. Garbin, C. Di Natali, J. Buzzi, E. De Momi, and P. Valdastri, "Laparoscopic Tissue Retractor Based on Local Magnetic Actuation," *Journal of Medical Devices*, vol. 9, no. 1, 2015.

[18] N. Garbin, P. R. Slawinski, G. Aiello, C. Karraz, and P. Valdastri, "Laparoscopic Camera Based on an Orthogonal Magnet Arrangement," *IEEE Robotics and Automation Letters*, vol. 1, pp. 924–929, 2016.

[19] S. Makita, C. Science, K. Ikuta, and S. Arimoto, "Non-contact magnetic gear for micro transmission mechanism," *Micro Electro Mechanical Systems, 1991, MEMS '91, Proceedings. An Investigation of Micro Structures, Sensors, Actuators, Machines and Robots. IEEE*, pp. 125–130, 1991.

[20] C. Di Natali, J. Buzzi, N. Garbin, M. Beccani, and P. Valdastri, "Closed-Loop Control of Local Magnetic Actuation for Robotic Surgical Instruments," *IEEE Transactions on Robotics*, vol. 31, pp. 143–156, 2015.

[21] F. Leong, A. Mohammadi, Y. Tan, D. Thiruchelvam, C. Y. Lai, P. Valdastri, and D. Oetomo, "Disturbance Rejection in Multi-DOF Local Magnetic Actuation for Robotic Abdominal Surgery," *IEEE Robotics and Automation Letters*, pp. 1568–1575, 2017.

[22] G. Hostetter and J. Meditch, "On the generalization of observers to systems with unmeasurable, unknown inputs," *Automatica*, vol. 9, no. 6, pp. 721–724, 1973.

[23] A. Radke and Zhiqiang Gao, "A survey of state and disturbance observers for practitioners," *2006 American Control Conference*, 2006.

[24] M. Bodson, "Rejection of periodic disturbances of unknown and time-varying frequency," *International Journal of Adaptive Control and Signal Processing*, vol. 19, no. 2-3, pp. 67–88, mar 2005.

[25] S. Sastry, M. Bodson, and J. F. Bartram, "Adaptive Control: Stability, Convergence, and Robustness," *The Journal of the Acoustical Society of America*, vol. 88, no. 1, pp. 588–589, jul 1990.

[26] P. Gahinet, A. Nemirovskii, A. Laub, and M. Chilali, "The LMI control toolbox," *Proceedings of 1994 33rd IEEE Conference on Decision and Control*, vol. 3, no. May 1995, pp. 2038–2041, 1994.